Experimental Thermal and Fluid Science 155 (2024) 111173

Contents lists available at ScienceDirect

Experimental Thermal and Fluid Science

journal homepage: www.elsevier.com/locate/etfs

Two-phase air-water measurements in fully-rough free-surface flows

Jiayue Hu , Hubert Chanson *

The University of Queensland, School of Civil Engineering, Brisbane, QLD 4072, Australia

ARTICLE INFO

Keywords:
Two-phase flow measurements
Free-surface flows
Fully-rough turbulent flows
Interfacial properties
Physical modelling

ABSTRACT

Fully-rough turbulent free-surface flows are encountered in a variety of natural and man-made applications. When strong turbulence interacts with the water surface, the intense air–water mixing yields a complicated two-phase gas–liquid flow structure due to the cumulative contribution of entrained bubbles and droplets. This study presents an in-depth investigation of fully-rough turbulent free-surface flows, through some experimental measurements in high-velocity free-surface flows over macro-roughness. The measurements focused on skimming flow conditions. Downstream of the inception region of self-aeration, some strong air entrapment and intense turbulence was recorded. The void fraction profiles compared well with a theoretical model, and the relationship between void fraction and bubble count rate exhibited a quasi-parabolic profile. The interfacial velocity distributions followed a power law, while high turbulence levels were recorded across the air–water column. A large proportion of clustered particles was observed in both the lower bubbly flow region and upper spray region, with a strong correlation between the percentage of clustered particles and void/liquid fraction.

1. Introduction

Free-surface flows represent a central issue in many natural, biological and industrial fields. Fully-rough turbulent free-surface flows are encountered in a variety of natural and man-made applications [44,13,62]. Civil and environmental engineering applications include mountain streams, bedrock rivers, artificial cascades, storm waterways, and dam spillways. These free-surface flows are most often characterised by strong air–water mixing at the free-surface, called “white waters” [51,67,12] (Fig. 1). Fig. 1A shows the white waters on an unlined rock cascade. Fig. 1B highlights the self-aeration in an artificial cascade fountain in front of the Taipei 101 building. Fig. 1C presents a large dam stepped spillway in operation during a major flood. Air entrainment in free-surface flows is ubiquitous in macro-roughness channels [25,50,68]. Air bubble entrapment requires large turbulent shear stresses acting next to the water surface to overcome both surface tension and buoyancy effects [73,74]. Experimental observations indicated that the turbulent free-surface flows exhibit some surface ’waves’ with small-scale eddies and larger underlying vortices, and air–water mixing is caused by the action of high intensity turbulent shear close to the water surface [66,16].

When strong turbulence interacts with an air–water surface, a number of different manifestations may occur, including the generation of surface waves, projections, cusps and dimple to surface breakup with formation of bubbles, drops and fully-mixed two-phase flows [8]. The mass transfer between air and water is drastically augmented by the combination by the large interfacial area in the air–water flow, the longer residence time, compared to smooth turbulent flows, and the fully-rough turbulent mixing [57,45]. The intense air–water mixing yields an increased gas–liquid interfacial area due to the cumulative surface area of both bubbles and droplets, and this makes the problem of turbulent gas–liquid multiphase flow far more complex than its single-phase counterpart [61,6]. A challenging issue is the limited amount of detailed validation data sets [53,3].

When the bubble entrapment is sizeable, e.g. as in Fig. 1, a dominant feature of the two-phase flow is turbulence modulation and coupling. Turbulence modulation by entrained particles (bubbles, droplets) may be caused by a number of mechanisms, including enhanced dissipation due the presence of particles, transfer of kinetic energy to the fluid from the bubbles, formation of wakes and vortex shedding behind the particles, and a combination of these mechanisms [3]. The influence of turbulence on the entrained air and surrounding atmosphere cannot be ignored and encompass air entrapment, bubble collision, break-up and agglomeration, drop ejection, droplet transport, roller interfacial deformation. This is sometimes referred to as ’two-way coupling’ or even ’four-way coupling’ [28]. To date, limited data exists for quantifying the interfacial processes and air–water flow structure. due to the metrology limitations [37,26,60]. Rather, most previous investigations

* Corresponding author at: The University of Queensland, School of Civil Engineering, Brisbane, QLD 4072, Australia.
E-mail address: h.chanson@uq.edu.au (H. Chanson).

https://doi.org/10.1016/j.expthermflusci.2024.111173
Received 4 January 2024; Received in revised form 21 February 2024; Accepted 26 February 2024
Available online 28 February 2024

(A) (B)

(A) Unlined rock cascade at Bosméléac, France on 11 June 2022 (shutter speed: 1/8,000 s)

(B) Stepped cascade at entrance of Exhibition and Convention Centre, Tapei City, Taiwan on 14 November 2010 (shutter speed: 1/320 s)

(C)

(C) Skimming flow on Hinze Dam stepped spillway, Australia on 5 March 2022 - Flow direction from bottom left to top right, Re = 7×10^6, h = 1.5 m, θ = 51.3° (shutter speed: 1/8,000 s)

Fig. 1. Free-surface aeration in fully-rough free-surface flows (A) Unlined rock cascade at Bosméléac, France on 11 June 2022 (shutter speed: 1/8,000 s). (B) Stepped cascade at entrance of Exhibition and Convention Centre, Tapei City, Taiwan on 14 November 2010 (shutter speed: 1/320 s). (C) Skimming flow on Hinze Dam stepped spillway, Australia on 5 March 2022 - Flow direction from bottom left to top right, Re = 7×10^6, h = 1.5 m, θ = 51.3° (shutter speed: 1/8,000 s).

of self-aerated flows have been focused in limited time-averaged properties.

This paper aims to gain an in-depth understanding of fully-rough turbulent free-surface flows, and provides a validation data set to assess the effect of turbulence on the coupling between the two phases. This was achieved through some experimental measurements in high-velocity free-surface flows over macro-roughness, in which detailed two-phase flow measurements were undertaken.

2. Similarity, physical model and methodology

2.1. Presentation

Laboratory experiments and computational models are commonly used during the engineering design process to optimise the final design and to ensure a safe operation [31]. In the laboratory model, the flow properties must be similar to those in the full-scale system with a similarity of form, of motion and of forces [42]. The modelling approach must be developed based upon the fundamental principles of similitude and dimensional analysis [4,52]. With most free-surface flows, the gravity effects are important and a Froude similitude is implemented. Considering an air–water flow down a staircase rectangular prismatic channel (Fig. 2), the characteristic length scale for a Froude similitude is the critical flow depth $d_c = (q^2/g)^{1/3}$, with q the discharge flow rate per unit width, also called unit discharge of water, and g the gravity constant [34,15]. The dimensional analysis gives a series of dimensionless relationships in terms of the two-phase air–water flow properties, at a dimensionless location (x/d_c, y/d_c, z/d_c) in the self-aerated chute flow, as functions of the fluid and physical properties, the channel geometry and boundary conditions:

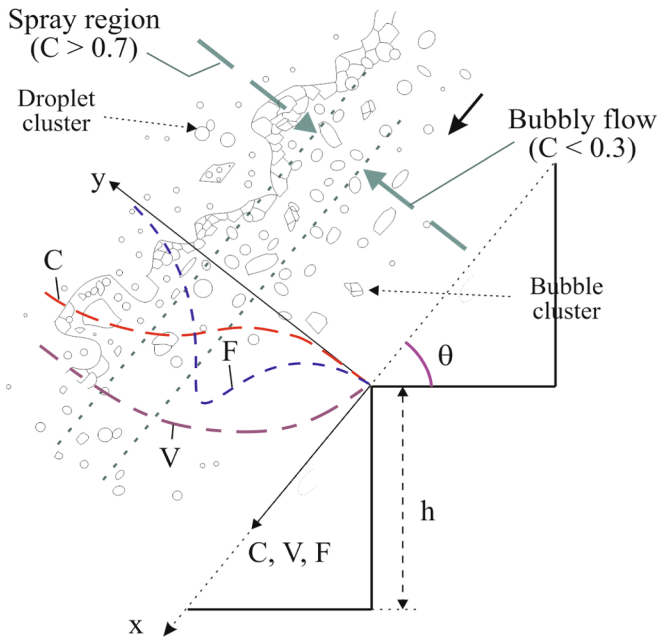

Fig. 2. Definition sketch of self-aerated fully-rough free-surface flow down a staircase invert.

$$C, \frac{V}{V_c}, \frac{F \times d_c}{V_c}, Tu, \frac{ch_p}{d_c}, \frac{N_c \times d_c}{V_c}, \ldots = F\left(\frac{x}{d_c}, \frac{y}{d_c}, \frac{z}{d_c}, \frac{B}{d_c}, \frac{k_s}{d_c}, \frac{h}{d_c}, \theta, \rho \times \frac{V_c \times d_c}{\mu}, \frac{\rho \times V_c^2 \times d_c}{\sigma}, \ldots\right) \quad (1)$$

where C is the local void fraction, V the interfacial longitudinal velocity component, V_c the characteristic velocity, called critical velocity, $V_c = (g \times d_c)^{1/2}$, F the bubble count rate, Tu a turbulence intensity, ch_p a characteristic air–water particle size, N_c the number of bubble clusters per second, x, y and z are respectively the longitudinal, normal and transverse coordinates, ρ and μ the water density and dynamic viscosity respectively, σ the surface tension between air and water, B the channel width, k_s the equivalent sand roughness height of the channel boundary surface, h the vertical step height, θ the angle between the invert and the horizontal (Fig. 2).

In Equation (1), right hand side, the 6th term is inversely proportional to a Froude number defined in terms of the vertical step height h, and the 8th and 9th terms are the Reynolds number and Weber number respectively. Since the Vaschy-Buckingham theorem implies that any non-dimensional parameter number could be replaced by a combination of other non-dimensional parameters and itself, the Weber number may be replaced by the Morton number Mo defined as [41,12]:

$$Mo = g \times \frac{\mu^4}{\rho \times \sigma^3} = \frac{We^3}{Re^4 \times Fr^2} \quad (2)$$

Herein, the same fluids, air and water, are used in laboratory and at full-scale, and the Morton number is an invariant. Further, the experiments were performed in a channel of constant width B with smooth surface roughness ($k_s \approx 0$) and constant chute slope θ. For the present air–water free-surface flow study, Equation (1) may be simplified as:

$$C, \frac{V}{V_c}, \frac{F \times d_c}{V_c}, Tu, \frac{ch_p}{d_c}, \frac{N_c \times d_c}{V_c}, \ldots = F\left(\frac{x}{d_c}, \frac{y}{d_c}, \frac{z}{d_c}, \frac{h}{d_c}, \rho \times \frac{V_c \times d_c}{\mu}, \ldots\right) \quad (3)$$

With a combined Froude and Morton similarity, and a physical model smaller than the prototype structure, the Reynolds number may be significantly smaller than at full-scale [47,48]. Herein, new experiments were repeated with an identical Froude and Morton number in a relatively large channel. The experimental configuration corresponded to Reynolds number $0.95 \times 10^5 < Re < 2 \times 10^5$ comparable to, or larger than, that of prototype free-surface flows commonly seen in cascades (Fig. 1A and 1B), man-made storm waterways and water treatment plants.

2.2. Physical model and instrumentation

The physical experiments were conducted in a stepped chute experiment located at the University of Queensland (UQ). The water was delivered by three pumps feeding a 1.7 m deep and 5 m wide concrete basin. The flow from the basin was smoothly converged into a symmetrical sidewall convergent before entering the 0.985 m wide test section. The convergent ensured a smooth and waveless flow into the upstream broad-crested weir. The crest controlled the flow over the 1.4 m high stepped chute, equipped with 0.10 m high, 0.08 m long and 0.985 m wide steps made of smooth PVC. The facility had the same slope as and was a simplified 1:15 scale model of the Hinze Dam stepped spillway, Australia seen in Fig. 1C.

The flow rate was calculated based upon the measured head above crest using a carefully-calibrated weir equation [22]. The clear-water flow depths were recorded with pointer gauge mounted over the channel centreline. The two-phase gas–liquid flow measurements were performed using a dual-tip phase-detection probe designed, developed and manufactured at the University of Queensland. The probe was equipped with two identical needle tip (∅0.25 mm) separated by a longitudinal distance Δx = 9.0 mm. Each needle tip signal was recorded for 45 s at 20 kHz. The two-phase flow properties were measured at several cross sections in the air–water flow region. The translation of the phase-detection probe in the direction normal of the chute slope was made with a Mitutoyo™ digital scale unit with accuracy of ± 0.025 mm. Visual observations were conducted with two dSLR cameras, Pentax™ K-3 (24 Mpx) and Pentax™ K-3iii (26 Mpx), equipped with professional-grade prime lenses with negligible lens distortion and a Casio™ EX-10 Exilim camera recording movies at 120 fps and 240 fps.

2.3. Signal processing

The needle tip signals were post-processed using a single threshold

Table 1
Experimental flow conditions.

Reference	θ (°)	B (m)	h (m)	Q (m^3/s)	d_c (m)	h/d_c (m)	Re	Instrumentation
Present study	51.3	0.985	0.10					
Visual observations				0.005 to 0.199	0.014 to 0.16	0.6 to 7	5×10^3 to 2×10^5	Video cameras and dSLR cameras
Two-phase flow measurements				0.094	0.098	1.02	0.94×10^5	Dual-tip phase-detection probe
				0.150	0.133	0.75	1.51×10^5	(Ø = 0.25 mm)
				0.193	0.158	0.63	1.95×10^5	

Notes: B: rectangular channel breadth; d_c: critical flow depth; h: upstream gate opening; Q: water discharge; Re: Reynolds: $Re = \rho \times V_c \times d_c/\mu$; θ: chute slope; For all experiments, phase-detection probe signal outputs sampled at 20 kHz per sensor for 45 s.

(A, Left) Flow above the broad-crest weir - Q = 0.150 m^3/s, h/d_c = 0.75, Re = 1.51×10^5

(B, Right) Air-water flow down the staircase chute - Q = 0.193 m^3/s, h/d_c = 0.63, Re = 1.95×10^5

Fig. 3. Experimental channel (flow direction from right to left). (A, Left) Flow above the broad-crest weir - Q = 0.150 m^3/s, h/d_c = 0.75, Re = 1.51×10^5. (B, Right) Air-water flow down the staircase chute - Q = 0.193 m^3/s, h/d_c = 0.63, Re = 1.95×10^5.

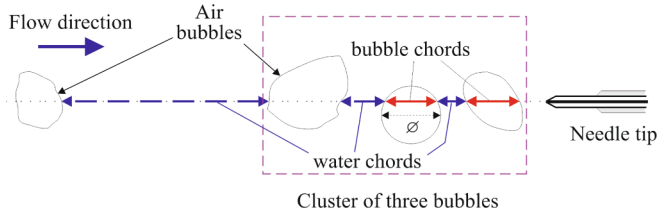

Fig. 4. Schematic of particle cluster detection by a phase-detection probe in dispersed air–water flow.

technique set at 50 % of the air–water voltage [11,58]. The time-averaged void fraction C was equal to the average time spent by the needle in air relative to the total sampling time. The bubble count rate F was the average number of detected particles (i.e. bubbles or droplets) per unit time [54,18]. The interfacial velocity V was derived from a cross-correlation technique, based upon the time lag corresponding to the maximum cross-correlation coefficient between leading and trailing needle signals [35,9,26]. The interfacial turbulence intensity Tu, defined as the ratio of rms velocity to time-averaged velocity, was deduced from the broadening of the cross-correlation function relative to the auto-correlation function [39,24].

The identification of particle clusters was undertaken based upon the analysis of the water/air chord between two successive bubbles/droplets detected by the lead sensor (Fig. 4). Herein, two adjacent particles were considered part of a cluster when the trailing particle was in the near wake of the lead particle [20]. For a bubble flow, the water chord between two adjacent bubbles was compared to the chord of the lead bubble such as:

$$t_{ch-w} < \lambda \times t_{ch-a} \quad (4)$$

where $t_{ch\text{-}w}$ is the water chord time and $t_{ch\text{-}a}$ is the chord time of the leading bubble. The coefficient λ was taken as unity following the sensitivity analysis of Sun and Chanson [55]. Fig. 4 presents an example of three-bubbles cluster detected by the needle tip. The near wake clustering detection method is considered to be robust as it is based upon a comparison between local two-phase flow time scales [32].

2.4. Experimental flow conditions

The experiments were conducted for water discharges between 0.005 m^3/s and 0.198 m^3/s (Table 1). Visual observations were performed for dimensionless ration h/d_c between 0.6 and 7, corresponding to Reynolds numbers within $0.5 \times 10^4 < Re < 2 \times 10^5$, with $Re = \rho \times V_c \times d_c/\mu$. Detailed two-phase flow measurements were undertaken for three dimensionless ratios h/d_c, corresponding to Reynolds numbers within $0.94 \times 10^5 < Re < 1.95 \times 10^5$ (Table 1). The flow conditions corresponded to a skimming flow pattern.

3. Basic flow features

Visual observations were undertaken for a wide of discharges (Table 1). With small discharges, i.e. $h/d_c > 2.2$, the flow presented a series of free-falling nappes, taking off at each step and impacting on downstream step. For a range of intermediate flow, i.e. $1.1 < h/d_c < 2.2$, the flow motion was chaotic and some strong splashing and spray was observed. For large flow rates, i.e. $h/d_c < 1.1$, the water skimmed over the pseudo-invert formed by the step edges. The mainstream was parallel to the pseudo-invert, as seen in Fig. 3B. This was a skimming flow regime, also called quasi-smooth or tranquil flow [46,40].

In skimming flows, a turbulent boundary layer developed downstream of the spillway crest, and the free surface appearance varied longitudinally (Fig. 5A). When the outer edge of the developing boundary layer started to interact with the water-surface, the turbulent Reynolds stresses acting in the vicinity of the water surface overcame the surface tension and buoyancy effects, and self-aeration took place with the sudden appearance of “white waters” [73,29,16]. The inception region of free-surface aeration was characterised by intense free-surface turbulence with rapidly-varied flow properties, in line with the relevant literature based upon laboratory and prototype observations on steep slopes [71,19]. Downstream of the inception region, the flow was aerated and the air–water mix presented a white appearance (Fig. 5). In the experimental channel, some strong recirculation was observed in each step cavity through the glass sidewalls, with irregular ejections of

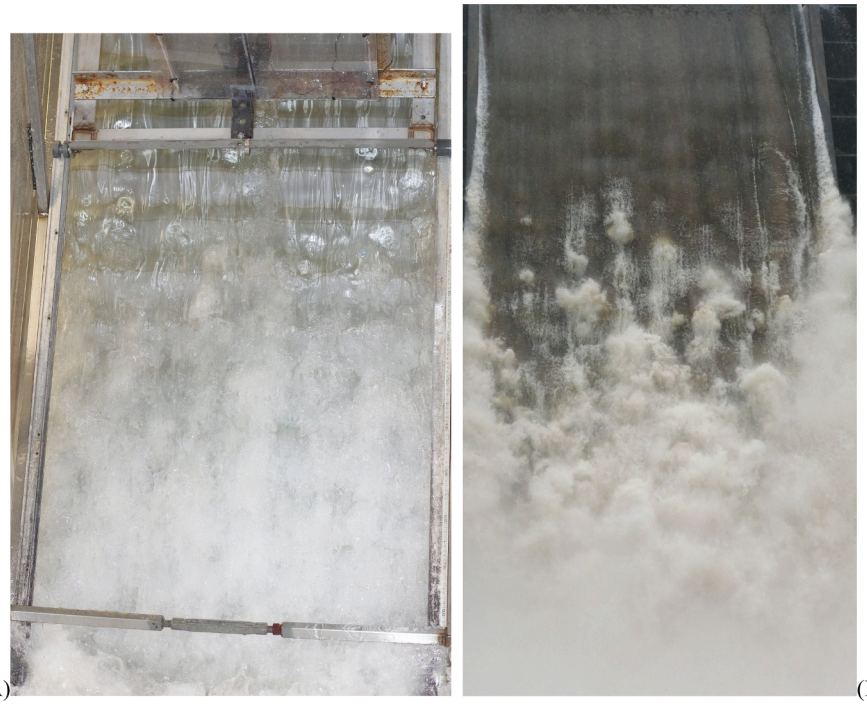

(A) (B)

Fig. 5. Air-water skimming flow down 51.3° staircase chutes under Froude similar conditions ($h/d_c = 0.63$), with flow direction from top to bottom - (A) Laboratory channel, $Q = 0.193\ m^3/s$, $h = 0.1\ m$, $h/d_c = 0.63$, $Re = 1.95 \times 10^5$, shutter speed: 1/100 s; (B) Hinze dam stepped spillway, $Q = 143\ m^3/s$, $h = 1.5\ m$, $h/d_c = 0.63$, $Re = 1.16 \times 10^7$, shutter speed: 1/640 s.

fluid out of the cavity into the main flow combined with some replacement of cavity fluid near the step edge, in a manner similar to d-type roughness cavity flow motion [27].

A visual comparison between the laboratory flow and Froude-similar prototype flow is shown in Fig. 5, in which the prototype has the same slope and is 15 times larger than the laboratory chute. In Fig. 5, the caption lists the respective flow conditions. Qualitatively, the physical experiments presented a similar appearance to the prototype overflow. There were however some key differences, namely (a) the extreme brightness of the air–water flow in the prototype, and (b) the intense nature of air–water turbulence in the self-aerated flow region of the prototype spillway (Fig. 5B). The first point was qualitatively and quantitatively documented through the exposure and white balance settings of the dSLR cameras. The brightness of the air–water flow at the Hinze Dam stepped spillway generated high to very-high light values (LVs), including during overcast and heavy rain episodes. These LV changes were difficult to predict and could happen rapidly within the ambient atmospheric conditions. The second point suggested a very dynamic air entrainment process in the prototype chute, combined with energetic bubble-turbulence two-way coupling. The finding implied that the air bubble diffusion process in laboratory might not be in true similitude with that in large prototype spillways, as previously discussed [12,71].

4. Two-phase air-water flow measurements

4.1. Void fraction data

In the air–water flow region, the two-phase flow properties were recorded at all step edges. In the direction y normal to the main stream, the measurements were obtained above the pseudo-bottom formed by the step edges up to the upper spray area. Typical results are presented in Figs. 6, 7, 8 and 9, where Y_{90} is the characteristic distance where the void fraction equals 90 %, V_{90} is the characteristics air–water velocity at $y = Y_{90}$, and F_{max} is the maximum bubble count rate in the section.

At each step edge, the void fraction profiles followed an inverted S-shape, illustrated in Fig. 6A. The void fraction distributions compared favourably to the advective diffusion theoretical model:

$$C = 1 - \tanh^2\left(K - \frac{y'}{2 \times D_o} + \frac{\left(y' - 1/3\right)^3}{3 \times D_o}\right) \quad (5)$$

with $y' = y/Y90$, and D_o a function of the depth-averaged void fraction and related to the dimensionless turbulent diffusivity D' [24]:

$$D' = \frac{D_o}{1 - 2 \times \left(y' - 1/3\right)^2} \quad (6)$$

The void fraction data highlighted a strong flow aeration and air–-water turbulent mix of the skimming flow, characterised by increased aeration with increasing distance downstream from the inception region of free-surface aeration. This is illustrated by the increased slope of void fraction distributions shown in Fig. 6A. At the downstream end of the stepped chute, the depth-averaged void fraction was about 40 % for all three flow conditions.

4.2. Bubble count rate data

The fragmentation of the air–water flow was quantified by the bubble count rate (Fig. 6B and 7). At each step edge, the bubble count rate profiles exhibited a marked maximum F_{max} (Fig. 6B). The relationship between void fraction and bubble count rate presented a pseudo-parabolic shape, although it was skewed, reaching a maximum for void fraction between 0.35 and 0.5 [59], as illustrated in Fig. 7A. All the data indicated an increasing maximum bubble frequency with increasing longitudinal distance without reaching an asymptotic value (Fig. 7B). This is seen in Fig. 7B. The finding is important as it unequivocally demonstrated that the two-phase flow structure, hence the bubble-turbulence interactions, evolved along the chute and did not reach an equilibrium before the downstream end of the channel. This

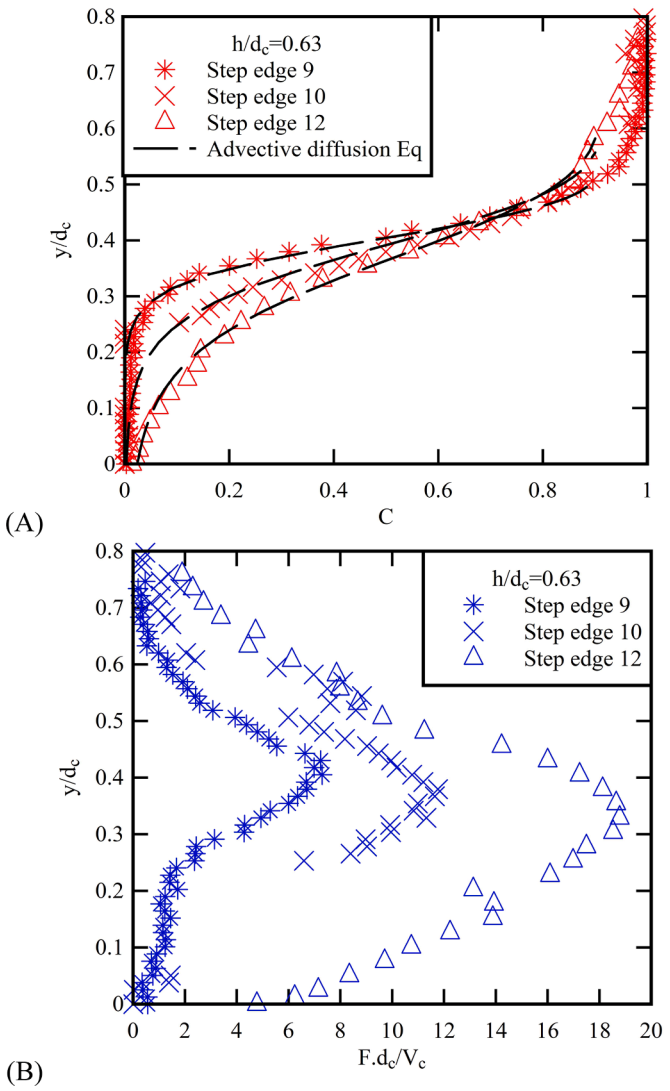

Fig. 6. Dimensionless distributions of (A) void fraction and (B) bubble count rate in the experimental channel - Comparison between void fraction data and Equation (5) (thick dashed lines) - Flow conditions: $Q = 0.193\ m^3/s$, $h/d_c = 0.63$, $Re = 1.95 \times 10^5$.

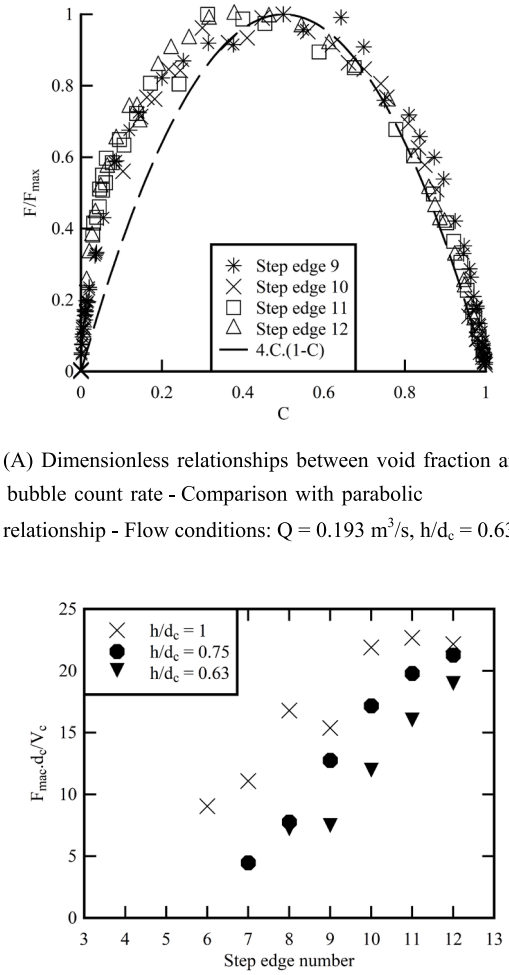

(A) Dimensionless relationships between void fraction and bubble count rate - Comparison with parabolic relationship - Flow conditions: $Q = 0.193\ m^3/s$, $h/d_c = 0.63$, $Re = 1.95 \times 10^5$

(B) Dimensionless longitudinal distributions of maximum bubble count rate

Fig. 7. Bubble count rate in air–water flows in the experimental channel. (A) Dimensionless relationships between void fraction and bubble count rate - Comparison with parabolic relationship - Flow conditions: $Q = 0.193\ m^3/s$, $h/d_c = 0.63$, $Re = 1.95 \times 10^5$. (B) Dimensionless longitudinal distributions of maximum bubble count rate.

longitudinal pattern might have some implication in terms of up-scaling the data and for model-prototype compliance [23,65].

4.3. Interfacial velocity and turbulence data

The interfacial velocity data showed some continuous air–water velocity distributions from the pseudo-bottom (i.e. $y = 0$) formed by the step edges up to the upper free-surface and 95 % to 99 % of void fraction. The experimental results compared favourably with a power law, for void fractions less than 90 %, and a quasi-uniform profile, above as shown in Fig. 8A:

$$\frac{V}{V_{90}} = y'^{1/N} \qquad 0 < y' < 1 \tag{7a}$$

$$\frac{V}{V_{90}} = 1 \qquad y' > 1 \tag{7b}$$

Herein, the inverse of power law exponent, i.e. N, varied between 3.5 and 6, comparable to earlier studies with similar boundary conditions [43,5]. The longitudinal variation of the characteristic air–water velocity data V_{90} highlighted the acceleration of the flow down the steep chute. The trend is presented in Fig. 8B, with H_1 the upstream total energy per unit mass, also called upstream total head. The current air–water flow data, in Fig. 8B, are compared with non-aerated surface velocity data V_s estimated from a theoretical solution of the Bernoulli principle [13], non-aerated flow measurements in laboratory [1,69] and quantitative observations at the Hinze Dam spillway seen in Fig. 1C and 5B [19]. In Fig. 8B, the results demonstrated that the effects of boundary resistance were nil on the free-surface velocity in the non-aerated developing flow region (Fig. 8B). Downstream of the inception region of free-surface aeration, the air–water velocity next to the upper surface was smaller than the ideal fluid flow estimate because of the effects of boundary friction and form drag caused by the triangular step cavities. Altogether, the overall trend is fascinating, with the complementary nature of theoretical estimates, laboratory data and prototype data.

The profiles of interfacial turbulence intensity Tu exhibited a relatively high turbulence level across the entire air–water column, i.e. $0 < y' < 1$ (Fig. 9A), typically larger than monophase flow values, e.g. Ohtsu and Yasuda [49], Amador [1], Zhang et al. [72,70]. The present values of interfacial turbulence intensity were of the similar order of magnitude as data in wake flows between rocks, separated flows past cavities, and surface turbulence in a smooth chute prototype spillway

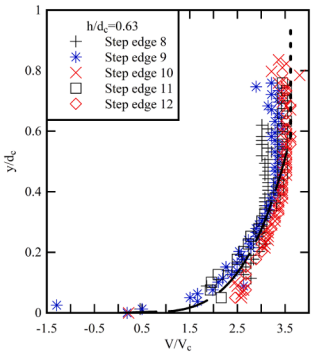

(A) Dimensionless distributions of interfacial velocity - Comparison with Equation (7) for N = 4 - Flow conditions: Q = 0.193 m^3/s, h/d_c = 0.63, Re = 1.95×10^5

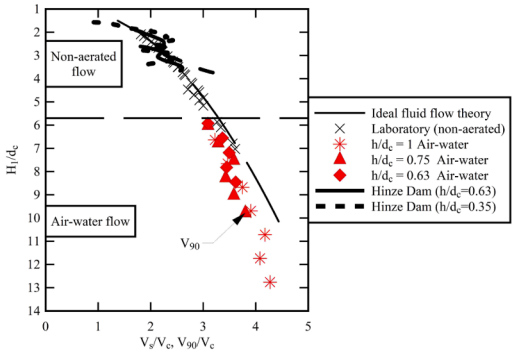

(B) Dimensionless longitudinal distribution of surface velocities in steep stepped chute: comparison betweennon-aerated surface velocity upstream of inception region (Theory, Laboratory data, Hinze Dam spillway prototype data) and characteristic air-water velocity V_{90}(Present data)

Fig. 8. Air-water velocity data in the experimental channel. (A) Dimensionless distributions of interfacial velocity - Comparison with Equation (7) for N = 4 - Flow conditions: Q = 0.193 m^3/s, $h/d_c = 0.63$, $Re = 1.95 \times 10^5$. (B) Dimensionless longitudinal distribution of surface velocities in steep stepped chute: comparison between non-aerated surface velocity upstream of inception region (Theory, Laboratory data, Hinze Dam spillway prototype data) and characteristic air–water velocity V_{90} (Present data).

[21]. At each step edge and for all flow rates, the relationship between turbulence intensity Tu and specific interfacial area a presented a monotonic increase in turbulence intensity with increasing interfacial area (Fig. 9B).

$$Tu - Tu_{mono} \propto a^M \qquad 0 < y' < 1 \tag{8}$$

with Tu_{mono} a typical monophase flow turbulence level on macro-roughness and a the specific interfacial area. Herein, the present data hinted $Tu_{mono} \approx 0.25$ comparable to the monophase data on stepped channels [49,1,72,70](Fig. 9B). The specific interfacial area was estimated as $a = 4 \times F/V$ [14]. The definition is valid for bubbly flows and sprays, with spherical and ellipsoidal particles. In regions of intermediate void fractions (i.e. $0.3 < C < 0.7$), the flow structure is more complex and a is proportional to the number of air–water interfaces per unit length of air–water mixture.

Immediately downstream of the inception region, the present data suggested $M < 1$. Further downstream, the results implied $M \approx 1$ (Fig. 9B). The strong correlation between turbulence level and interfacial area was likely linked to bubble/droplet breakup processes resulting from turbulent interactions with eddies of similar length scales as the particle [70,72].

5. Bubbly flow structure

5.1. Bubble chord lengths

The phase-detection probe signal was analysed in terms of the streamwise air and water structures detected by the leading sensor to gain some sub-millimetric description of the air–water flow. Where the void fraction was less than 0.3, the dispersed phase was air and the carrier phase was water. Whereas, when the void fraction was greater than 0.7, the dispersed particles were water droplets. In regions of intermediate void fraction ($0.3 < C < 0.7$), the air–water flow structure was complicated and most difficult to characterise [30]. In the current study, the particle chord length was equal to the particle chord time times the interfacial velocity.

The particle chord length data highlighted a wide range of bubble and droplet chord sizes at each measurement location. All the particle size distributions were skewed with a preponderance of small particle chord lengths relative to the mean. In the bubbly flow region, the distributions of bubble chords closely followed a log-normal probability distribution function. The probability of bubble chord lengths was the largest for bubble sizes between 0 and 2.5 mm. Note however the amount of bubbles larger than 5 mm. In the spray region ($C > 0{:}7$), the water chord distributions exhibited some flatter and wider distributions. Fig. 10 (Left) shows air-bubble chord size distributions obtained in bubbly flow regions ($C < 0.3$) for three different flow conditions at the same step edge with similar void fraction. Fig. 10 (Right) presents some typical distributions of water-droplet chord sizes in the spray region ($C > 0.7$). In each graph, each data represents the probability of bubble/droplet chord length in 0.5 mm intervals. The last column indicates the probability of chord lengths larger than 20 mm. Altogether, the structure of the bubbly and spray flow recorded at step edges was relatively comparable for all flow conditions, in terms of the chord size distributions. In the upper spray region, the microscopic structure of the flow appeared little affected by the flow rate.

5.2. Bubble clustering

The streamwise particle clustering was carefully documented, since the particle clustering rate may serve as a proxy for the level of particle-turbulence interactions. Fig. 11 depicts typical probability density functions of cluster size, i.e. number of particles per cluster. Measurements were taken at the step edges in the bubbly zone (Fig. 11A) and the spray region (Fig. 11B). The results were overall comparable in terms of the number of particles identified and the proportion of particles forming clusters in the bubbly and spray zones. Altogether, the data revealed that an absolute majority of particle clusters comprised only two particles travelling one after other, with about 15 % consisting of three particles and 5 % consisting of four or more particles.

For all the data, the clustering properties were summarised in terms of the average cluster size N_{clu}, defined as the number of particles per cluster, with $N_{clu} \geq 2$, and the clustering rate P_{clu}, defined as the percentage of clustered particles relative to the total number of detected particles. Complete vertical distributions were obtained for $C < 0.3$ in the bubbly flow region and for $C > 0.7$ in the spray region, and the comparison between the bubble count rate and clustering rate profiles suggested a similar relationship. The results are shown in Fig. 12, in red for droplet clustering in the spray region ($C > 0.7$) and in blue for bubble clusters in the bubbly flow region ($C < 0.3$). More, the vertical distributions of both N_{clu} and P_{clu} showed some similarity with the profile shape of void/liquid fraction i.e. C and (1-C) respectively. Fig. 13A plots the clustering rate P_{clu} as a function of the local dispersed phase fraction for the data presented in Fig. 12. At the downstream end of the steep chute, the cluster rate data distributions showed:

$$P_{clu} \propto C^{\alpha} \qquad \text{bubble clusters} \quad -C < 0.3 \tag{9a}$$

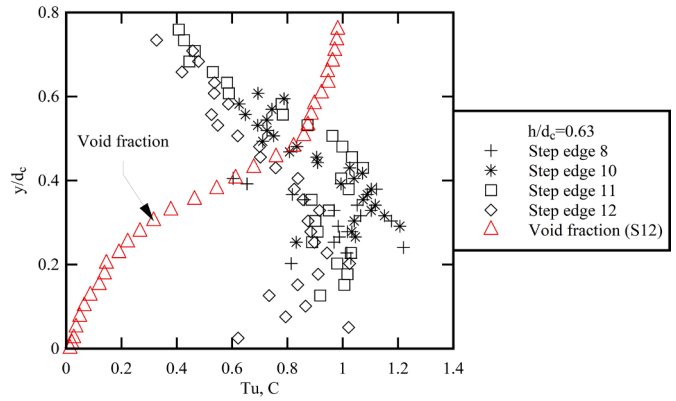

(A) Dimensionless profiles of turbulence intensity at step edges for Q = 0.193 m^3/s, h/d_c = 0.63, Re = 1.95×10^5 - Comparison with void fraction data step edge 12

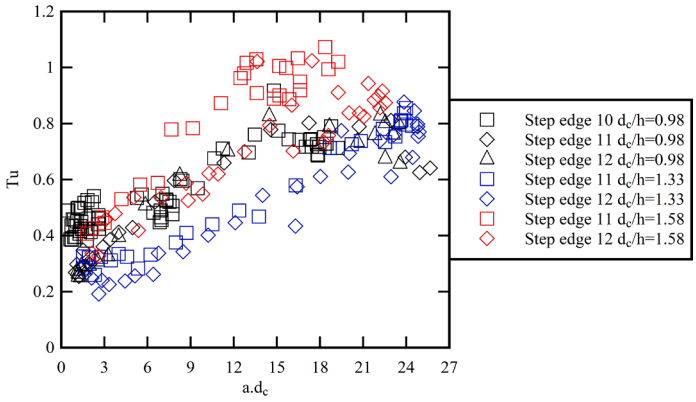

(B) Dimensionless relationship between turbulence intensity and specific interfacial area a

Fig. 9. Dimensionless distributions of interfacial turbulence intensity Tu in the experimental channel. (A) Dimensionless profiles of turbulence intensity at step edges for Q = 0.193 m^3/s, $h/d_c = 0.63$, Re = 1.95×10^5 - Comparison with void fraction data step edge 12. (B) Dimensionless relationship between turbulence intensity and specific interfacial area a.

$$P_{clu} \propto (1 - C)^{\beta} \qquad \text{droplet clusters} \quad -C > 0.7 \tag{9b}$$

independently of the flow conditions, with $\alpha \approx 0.3$ for $C < 0.3$ and $\beta \approx 0.55$ for $C > 0.7$. Such a trend indicated that an increase in local void/liquid fraction led to a larger proportion of particles being clustered and interacting with neighbouring particles.

Overall, in the self-aerated flows, the fraction of bubbles/droplets trapped in the cluster structures was considerable (Fig. 12 Left) and increased with void/liquid fractions. The number of particles in clusters also increased with increasing particle concentrations, i.e. void/liquid fractions (Fig. 12 Right). The accumulation of bubbles/droplets was enhanced with increasing interfacial area and turbulence intensity. Indeed, the turbulence intensity was found to increase as the particle volume fraction and specific interface area increased [36,25], Present study) (Fig. 9B). This led to a strong intensification of the clustering, encompassing a larger fraction of particles. Some key contrasted differences between air bubbles and water droplets include the compressibility of the gaseous particles and the inertia of the liquid particles. Due to inertial effects arising from the density contrast with the water phase, light particles could be expected to remain clustered for much longer times than the flow structures which cause the clustering [56].

5.3. Discussion

In two-phase turbulent flows, the dispersed and continuous phases can have a significant effect on the other phase's dynamics When particles are dispersed in turbulent flows at sufficiently high concentrations, the continuous/carrier phase and dispersed phase are two-way coupled [3]. The mutual transfer of momentum and energy between the two phases yields a modification of both the particle behaviour and flow turbulence. In one hand, the dispersed particles modify the turbulence in the carrier phase, while their behaviour may be profoundly affected. With increasing particle concentrations, hence void/liquid fractions, the particles become less able to respond to the carrier phase fluid flow fluctuations, and the random un-correlated component of their motion grows [10,33]. This translated into a positive correlation between the percentage of clustered particles P_{clu} and turbulence level Tu, illustrated in Fig. 13B and observed in the present study.

The present data set showed a relatively large proportion of clustered particles, despite a simplistic streamwise analysis which did not consider any two- and three-dimensional clustering [38,55,63]. The present longitudinal clustering detection method provided an underestimate of the "real" amount of clustered particles and number of particles per cluster [55]. In the present study, the fraction of bubbles/droplets trapped in cluster structures increased with void/liquid fractions. A positive correlation between clustering rates, turbulence levels and interfacial area was observed, in line with earlier self-aerated flow data sets [25,64]. The accumulation of bubbles/droplets was enhanced with increasing interfacial area and turbulence intensity. The finding was observed for a relatively wide range of invert roughness [2], Present study) and this result suggests the universality of this positive correlation relationship (Eq. (9)) in fully-rough self-aerated free-surface flows.

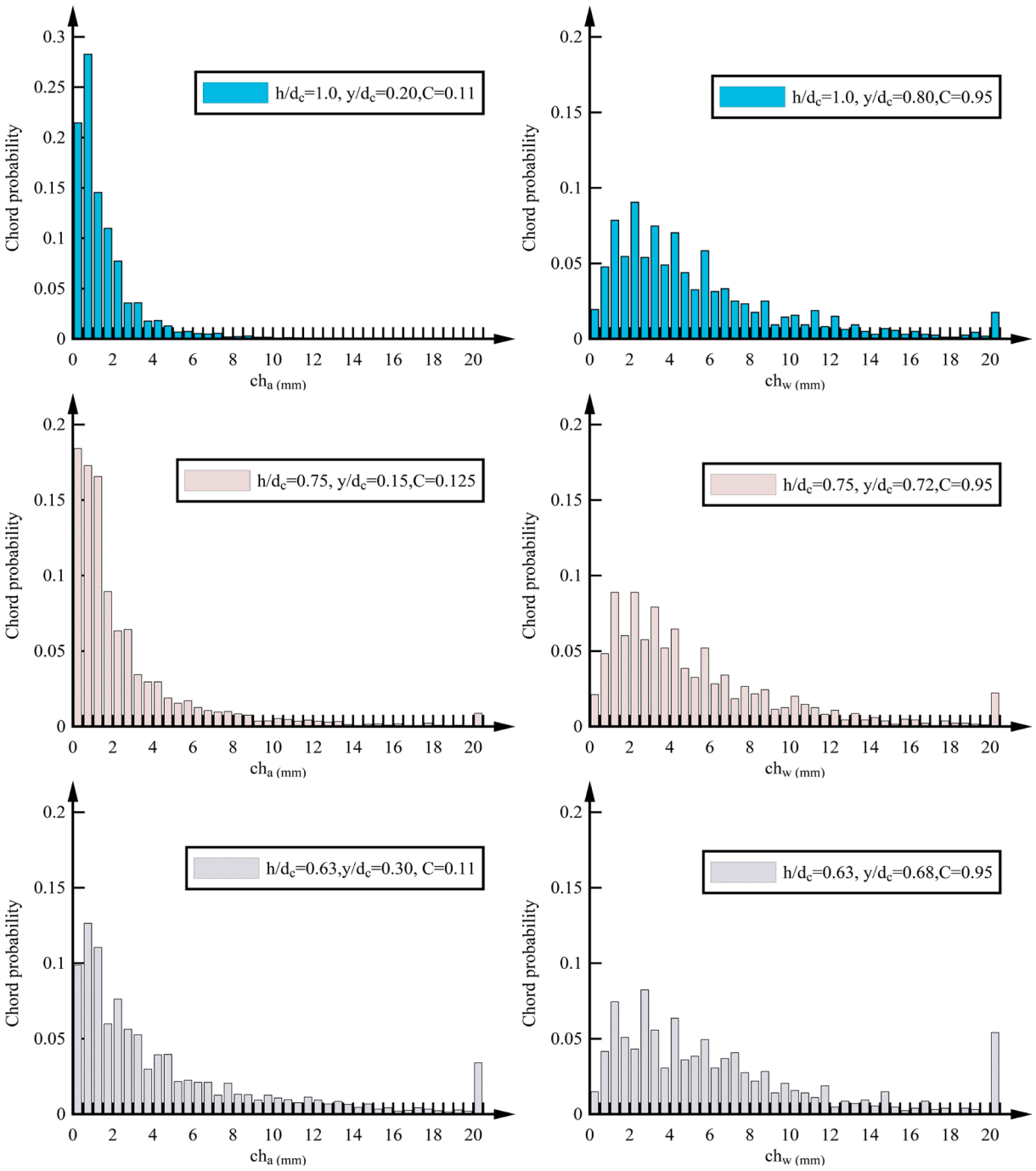

Fig. 10. Particle chord length distributions in the experimental channel (Left) Air chord lengths in the bubbly flow region for C ≈ 0.11 (Right) water chord lengths in the spray region for C ≈ 0.95.

6. Conclusion

The two-phase flow properties of self-aerated flows were investigated physically in a steep stepped channel. The thrust of the study was to deliver a robust characterisation of the un-controlled free-surface aeration in high-velocity free-surface flows over macroroughness. The physical measurements focused on skimming flow conditions. The upstream flow motion was accelerated and non-aerated. Downstream of the inception region of self-aeration, some strong air entrapment and intense turbulence was recorded. Detailed air–water flow measurements demonstrated that the void fraction profiles compared well with a theoretical model, that the relationship between void fraction and bubble count rate exhibited a quasi-parabolic profile, and that the interfacial velocity distributions followed a power law. High turbulence levels were recorded and provided quantitative evidence of complicated bubble-turbulence interactions and two-way coupling. The experimental results revealed a large proportion of clustered particles in both the lower bubbly flow region and upper spray region, with a preponderance of two-particle clusters. Some strong correlation between the percentage of clustered particles and void/liquid fraction was recorded.

Although the present measurements were conducted at relatively high Reynolds numbers ($0.94 \times 10^5 < \rho \times V_c \times d_c/\mu < 1.95 \times 10^5$), the physical model was smaller than some prototype hydraulic structures operating during major flood events with Reynolds numbers above 10^6 (e.g. Fig. 1C & 5B). Field measurements in such ultra-high Reynolds number free-surface flows presents a number of intrinsic challenges, that

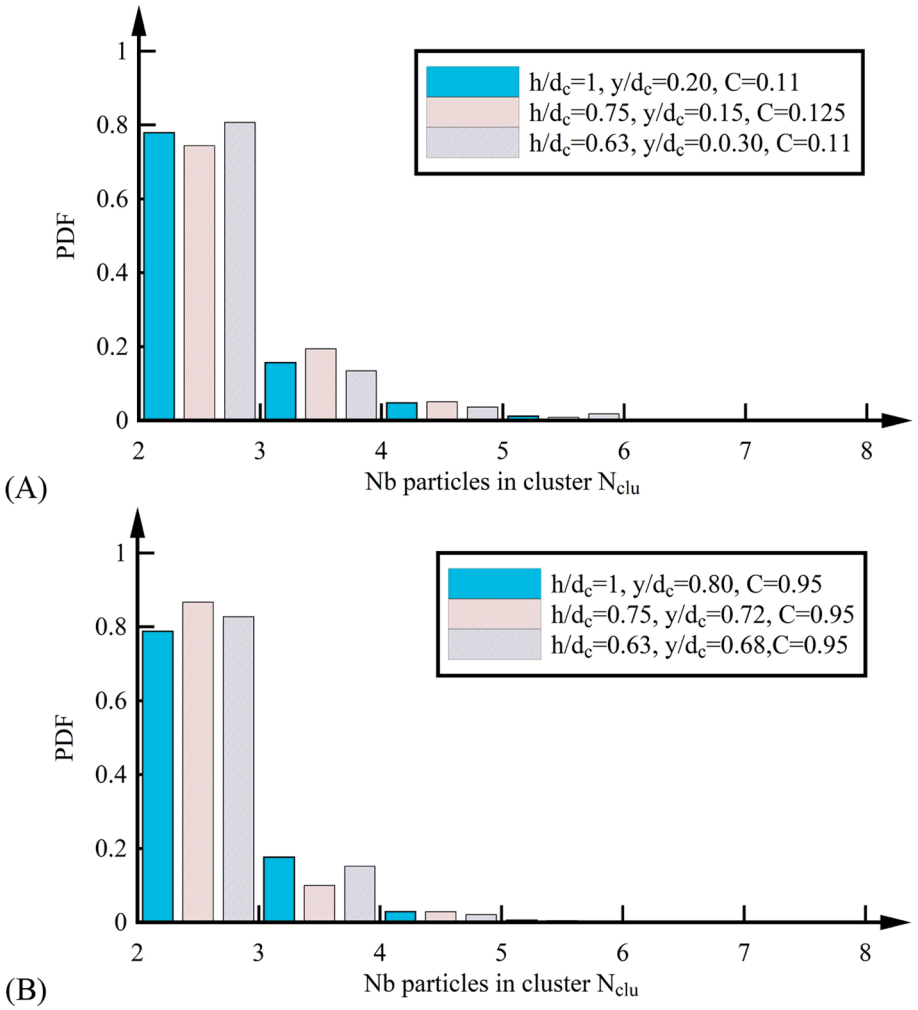

Fig. 11. Probability density functions of number of particles in clusters - (A) Clusters of bubbles; (B) Clusters of droplets.

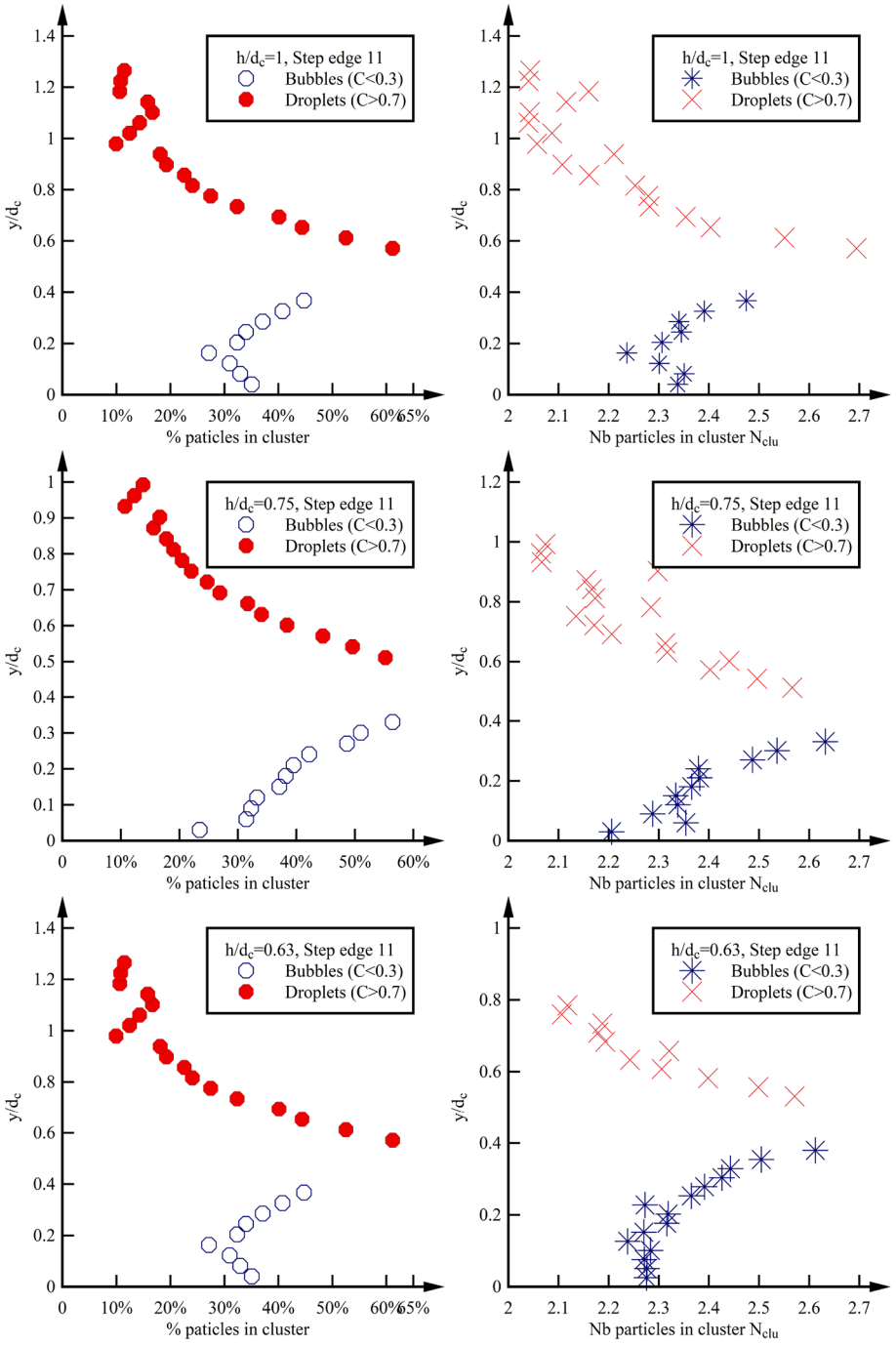

Fig. 12. Particle clustering in the experimental channel - (Left) Percentage of clustered particles; (Right) Average number of particles in clusters.

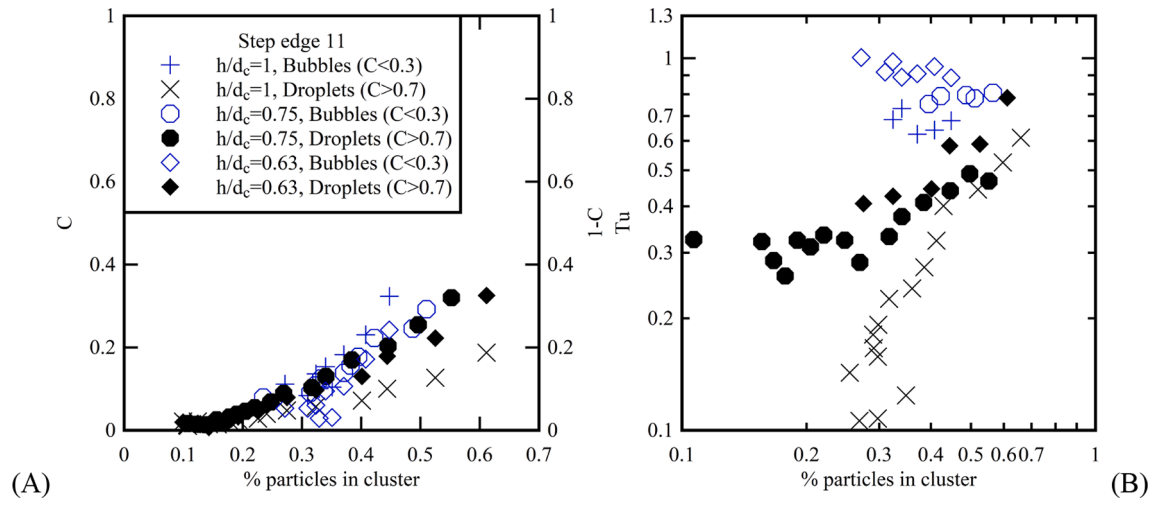

Fig. 13. Particle clustering characteristics - (A) Comparison between the percentage of clustered particles and local void/liquid fraction; (B) Comparison between the percentage of clustered particles and local turbulence intensity (Same legend for both graphs).

would require the development of ultimate two-phase flow metrology to obtain un-biased data sets (e.g. [21]. While beyond the scope of the present paper, a major challenge of many prototype self-aerated flows during major floods is the three-phase nature of these gas–liquid-solid flows advecting air, water and sediments [7,17].

CRediT authorship contribution statement

Jiayue Hu: Writing – review & editing, Visualization, Validation, Resources, Methodology, Investigation, Formal analysis, Data curation. **Hubert Chanson:** Writing – review & editing, Writing – original draft, Visualization, Validation, Supervision, Resources, Project administration, Investigation, Funding acquisition, Formal analysis, Conceptualization.

Declaration of competing interest

The authors declare that they have no known competing financial interests or personal relationships that could have appeared to influence the work reported in this paper.

Data availability

Data will be made available on request.

Acknowledgements

The authors acknowledge the technical assistance of Jason Van Der Gevel and Stewart Matthews (The University of Queensland). The financial support of the University of Queensland, School of Civil Engineering is acknowledged.

References

[1] A.T. Amador, Comportamiento Hidraulico de los Aliviaderos Escalonados en Presas de Hormigon Compactado. Ph.D. thesis, Univ. Polytech. of Catalunya, Barcelona, Spain, 2005, p. 204.
[2] R. Bai, Z. Bai, H. Wang, S. Liu, "Air-water mixing in vegetated supercritical flow: Effects of vegetation roughness and water temperature on flow self-aeration", Water Resour. Res. 58 (2022) 23, https://doi.org/10.1029/2021WR031692. Paper e2021WR031692.
[3] S. Balachandar, J.K. Eaton, Turbulent disperse multiphase flow, Annu. Rev. Fluid Mech. 42 (2010) 111–133.
[4] J. Bertrand, "Sur l'homogénéité dans les formules de physique", Comptes rendus 86 (15) (1878) 916–920.
[5] R.M. Boes, Zweiphasenströmung und Energieumsetzung an Grosskaskaden. ('Two-Phase Flow and Energy Dissipation on Cascades.') Ph.D. thesis, VAW-ETH, Zürich, Switzerland, 2000 (in German).
[6] F.A. Bombardelli, Computational multi-phase fluid dynamics to address flows past hydraulic structures, in: J. Matos, S. Pagliara, I. Meireles (Eds.), Proceedings of 4th IAHR International Symposium on Hydraulic Structures ISHS2012, APRH – Associação Portuguesa dos Recursos Hídricos [Portuguese water resources association], 9–11 February, Porto, Portugal, Keynote lecture (CD-ROM), 2012, p. 19.
[7] F. Bombardelli, H. Chanson, Progress in the observation and modeling of turbulent multi-phase flows, Environ. Fluid Mech. 9 (2) (2009) 121–123, https://doi.org/10.1007/s10652-009-9125-8).
[8] M. Brocchini, D.H. Peregrine, The dynamics of strong turbulence at free surfaces. Part 1. Description, J. Fluid Mech. 449 (2001) 225–254.
[9] P. Cain, I.R. Wood, Measurements of self-aerated flow on a spillway, Jl. Hyd. Div., ASCE 107 (HY11) (1981) 1425–1444.
[10] E. Calzavarini, T.H. van der Berg, F. Toschi, D. Lohse, "Quantifying microbubble clustering in turbulent flow from single-point measurements", Phys. Fluids 20 (4) (2008) 6, https://doi.org/10.1063/1.2911036. Paper 040702.
[11] A. Cartellier, J.L. Achard, Local phase detection probes in fluid/fluid two-phase flows, Rev. Sci. Instrum. 62 (2) (1991) 279–303.
[12] H. Chanson, Air Bubble Entrainment in Free-SurfaceTurbulent Shear Flows, Academic Press, London, UK, 1997, p. 401.
[13] H. Chanson, The Hydraulics of Stepped Chutes and Spillways, Balkema, Lisse, The Netherlands, 2001, p. 384.
[14] H. Chanson, Air-water flow measurements with intrusive phase-detection probes. Can we improve their interpretation? J. Hydraulic Eng., ASCE 128 (3) (2002) 252–255, https://doi.org/10.1061/(ASCE)0733-9429(2002)128:3(252)).
[15] H. Chanson, The Hydraulics of Open Channel Flow: An Introduction. Butterworth-Heinemann, second ed., Oxford, UK, 2004, p. 630.
[16] H. Chanson, Turbulent air-water flows in hydraulic structures: Dynamic similarity and scale effects, Environ. Fluid Mech. 9 (2) (2009) 125–142, https://doi.org/10.1007/s10652-008-9078-3.
[17] H. Chanson, "Hydraulics of aerated flows: Qui pro quo?", J. Hydraulic Res., IAHR, Invited Vision Pap. 51 (3) (2013) 223–243, https://doi.org/10.1080/00221686.2013.795917.
[18] H. Chanson, Phase-detection measurements in free-surface turbulent shear flows, J. Geophys. Eng. 13 (2) (2016) S74–S87, https://doi.org/10.1088/1742-2132/13/2/S74.
[19] H. Chanson, "On air entrapment onset and surface velocity in high-speed turbulent prototype flows", Flow Meas. Instrum. 83 (2022) 9, https://doi.org/10.1016/j.flowmeasinst.2022.102122. Paper 102122.
[20] H. Chanson, S. Aoki, A. Hoque, Bubble entrainment and dispersion in plunging jet flows: Freshwater versus seawater, J. Coastal Res. 22 (3) (2006 May) 664–677, https://doi.org/10.2112/03-0112.1.
[21] H. Chanson, C.J. Apelt, Environmental fluid mechanics of minimum energy loss weirs: Hydrodynamics and self-aeration at Chinchilla MEL Weir during the November-December 2021 flood event, Environ. Fluid Mech. 23 (3) (2023) 633–659, https://doi.org/10.1007/s10652-023-09926-0.
[22] N. Chaokitka, H. Chanson, Hydraulics of a broad-crested weir with rounded edges: physical modelling, in: Proceedings of 30th Hydrology and Water Resources Symposium HWRS2022, Brisbane, Australia, 30 November-2 December, Published by Engineers Australia, Brisbane, Australia, Paper 07, 2022, pp. 43–52.
[23] H. Chanson, C.A. Gonzalez, "Physical modelling and scale effects of air-water flows on stepped spillways", J. Zhejiang Univ.Sci. 6A (3) (2005 March) 243–250, https://doi.org/10.1007/BF02872325.

[24] H. Chanson, L. Toombes, Air-water flows down stepped chutes: Turbulence and flow structure observations, Int. J. Multiph. Flow 28 (11) (2002) 1737–1761, https://doi.org/10.1016/S0301-9322(02)00089-7.
[25] H. Chanson, L. Toombes, Strong interactions between free-surface aeration and turbulence in an open channel flow, Exp. Therm. Fluid Sci. 27 (5) (2003) 525–535, https://doi.org/10.1016/S0894-1777(02)00266-2.
[26] C. Crowe, M. Sommerfield, Y. Tsuji, Multiphase Flows with Droplets and Particles, CRC Press, Boca Raton, USA, 1998, p. 471.
[27] L. Djenidi, R. Elavarasan, R.A. Antonia, The turbulent boundary layer over transverse square cavities, J. Fluid Mech. 395 (1999) 271–294.
[28] S. Elgobashi, Particle-laden turbulent flows: direct simulation and closure models, Appl. Scient. Res. 48 (1991) 301–314.
[29] D.A. Ervine, H.T. Falvey, Behaviour of Turbulent Water Jets in the Atmosphere and in Plunge Pools, in: Proceedings of the Institution Civil Engineers, London, Part 2, Mar. 1987, 83, pp. 295–314. Discussion: Part 2, Mar.-June 1988, 85, 1987, pp. 359–363.
[30] S. Felder, H. Chanson, Air–water flow characteristics in high-velocity free-surface flows with 50% void fraction, Int. J. Multiph. Flow 85 (2016) 186–195, https://doi.org/10.1016/j.ijmultiphaseflow.2016.06.004.
[31] J.F. Foss, R. Panton, A. Yarin, Nondimensional Representation of the Boundary-Value Problem, in: C. Tropea, A.L. Yarin, J.F. Foss (Eds.), Springer Handbook of Experimental Fluid Mechanics, Springer, Part A, Chapter 2, 2007, pp. 33–82.
[32] C. Gualtieri, H. Chanson, "Effect of froude number on bubble clustering in a hydraulic jump", J. Hydraulic Res., IAHR 48 (4) (2010) 504–508, https://doi.org/10.1080/00221686.2010.491688.
[33] R. Hassaini, A.J. Petersen, F. Coletti, "Effect of two-way coupling on clustering and settling of heavy particles in homogeneous turbulence", J. Fluid Mech. 976 (2023) 21, https://doi.org/10.1017/jfm.2023.896. Paper A12.
[34] F.M. Henderson, Open Channel Flow, MacMillan Company, New York, USA, 1966.
[35] R.A. Herringe, M.R. Davis, Structural development of gas-liquid mixture flows, J. Fluid Mech. 73 (1976) 97–123.
[36] T. Hibiki, M. Ishii, Z. Xiao, Axial interfacial area transport of vertical bubbly flows, Int. J. Heat Mass Transf. 44 (2001) 1869–1888.
[37] O.C. Jones, J.M. Delhaye, Transient and statistical measurement techniques for two-phase flows: A critical review, Int. J. Multiph. Flow 3 (1976) 89–116.
[38] I. Kataoka, M. Ishii, A. Serizawa, Local formulation and measurements of interfacial area concentration in two-phase flow, Int. J. Multiph. Flow 12 (4) (1986) 505–529.
[39] H. Kipphan, F. Mesch, Flow Measurements using Transit Time Correlation. Flow Measurements of Fluids, in: H.H. Dijstelbergen, E.A. spencer (Eds.), North Holand Publ. Co., 1978, pp. 409–416.
[40] D.W. Knight, J.A. Macdonald, "Hydraulic resistance of artificial strip roughness", J. Hydraulic Div., ASCE 105 (HY6) (1979 June) 675–690.
[41] H. Kobus, Local Air Entrainment and Detrainment, in: H. Kobus (Ed.), Proceedings International Symposium on Scale Effects in Modelling Hydraulic Structures, IAHR, Esslingen, Germany, Paper 4.10, 1984, p. 10.
[42] J.A. Liggett, Fluid Mechanics, McGraw-Hill, New York, USA, 1994.
[43] J. Matos, Emulsionamento de ar e dissipação de energia do escoamento em descarregadores em degraus. ('Air entrainment and energy dissipation in flow over stepped spillways.') Ph.D. thesis, IST, Lisbon, Portugal, 1999 (in Portuguese).
[44] J.S. Montes, Hydraulics of Open Channel Flow, ASCE Press, New-York, USA, 1998, p. 697.
[45] D.B. Moog, G.H. Jirka, Stream Reaeration in nonuniform flow: Macroroughness enhancement, J. Hydraul. Eng., ASCE 125 (1) (1999) 11–16.
[46] H.M. Morris, Hydraulics of energy dissipation in steep, rough channels. Bulletin No. 19, Virginia Polytechnic Institute, Blacksburg, USA, 1968, p. 108.
[47] P. Novak, J. Cabelka, Models in Hydraulic Engineering. Physical Principles and Design Applications, Pitman Publ, London,UK, 1981, p. 459.
[48] P. Novak, V. Guinot, A. Jeffrey, D.E. Reeve, "Hydraulic Modelling - an Introduction", CRC Press, Taylor & Francis, London, UK, 2010, p. 599.
[49] I. Ohtsu, Y. Yasuda, Characteristics of Flow Conditions on Stepped Channels, in: Proc. 27th IAHR Biennial Congress, San Francisco, USA, Theme D, 1997, pp. 583–588.
[50] G.B. Pasternack, C.R. Ellis, J.D. Marr, Jet and hydraulic jump near-bed stresses below a horseshoe waterfall, Water Resour. Res. 43 (2007) 14. Paper W07449.
[51] N.S.L. Rao, H.E. Kobus, Characteristics of Self-Aerated Free-Surface Flows. Water and Waste Water/Current Research and Practice, vol. 10, Eric Schmidt Verlag, Berlin, Germany, 1974, p. 224.
[52] H. Rouse, Fluid Mechanics for Hydraulic Engineers, McGraw-Hill Publ, New York, USA, 1938 (also Dover Publ., New York, USA, 1961, 422 pages).
[53] P. Sagaut, S. Deck, L. Larcheveque, Numerical Simulation Data: from Validation to Physical Analysis, in: J.M. Most, L. David, F. Penot, L.E. Brizzi (Eds.), Proc. 11ème Congrès Francophone de Techniques Laser CFTL 2008, Poitiers Futuroscope, France, 16-19 Sept., Invited plenary, 2008, pp. 29–43 (ISBN 2-905267-62-3).
[54] A. Serizawa, Fluid-Dynamic Characteristics of Two-Phase Flow. Ph.D. thesis, Institute of Atomic Energy, Kyoto University, Japan, 1974.
[55] S. Sun, H. Chanson, Characteristics of clustered particles in skimming flows on a stepped spillway, Environ. Fluid Mech. 13 (1) (2013) 73–87, https://doi.org/10.1007/s10652-012-9255-2.
[56] Y. Tagawa, J.M. Mercado, V.N. Prakash, E. Calzavarini, C. Sun, D. Lohse, Three-dimensional Lagrangian Voronoï analysis for clustering of particles and bubbles in turbulence, J. Fluid Mech. 693 (2012) 201–215, https://doi.org/10.1017/jfm.2011.510.
[57] K. Toda, K. Inoue, Advection and Diffusion properties of Air Bubbles in Open Channel Flow, in: F.M. Holly Jr., A. Alsaffar (Eds.), Proc. 27th IAHR Congress, San Francisco, USA, Theme B, vol. 1, 1997, pp. 76–81.
[58] L. Toombes, Experimental Study of Air-Water Flow Properties on Low-Gradient Stepped Cascades. Ph.D. thesis, Dept of Civil Engineering, The University of Queensland, Brisbane, Australia, 2002.
[59] L. Toombes, H. Chanson, Interfacial aeration and bubble count rate distributions in a supercritical flow past a backward-facing step, Int. J. Multiph. Flow 34 (5) (2008) 427–436, https://doi.org/10.1016/j.ijmultiphaseflow.2008.01.005.
[60] C. Tropea, A.L. Yarin, J.F. Foss, Springer Handbook of Experimental Fluid Mechanics, Springer, Berlin, Germany, 2007, p. 1557.
[61] G. Tryggvason, R. Scardovelli, S. Zaleski, Direct Numerical Simulations of Gas-Liquid Multiphase Flows, Cambridge University Press, Cambridge, UK, 2011, p. 338.
[62] B.L. Valle, G.B. Pasternack, "Air concentrations of submerged and unsubmerged hydraulic jumps in a bedrock step-pool channel", J. Geophys. Res. 111 (F3) (2006) 12, https://doi.org/10.1029/2004JF000140, paper F030l6.
[63] H. Wang, Z. Hu, H. Chanson, Two-dimensional bubble clustering in hydraulic jumps, Exp. Therm. Fluid Sci. 68 (2015) 711–721, https://doi.org/10.1016/j.expthermflusci.2015.07.006.
[64] H. Wang, X. Liu, R. Bai, S. Liu, "Bubble characteristics affecting air-water exchange in open-channel flow with a jet forming over a sudden bottom drop", Exp. Therm. Fluid Sci. 124 (2021) 11, https://doi.org/10.1016/j.expthermflusci.2021.110366. Paper 110366.
[65] H. Wang, Z. Bai, X. Liu, R. Bai, S. Liu, Flow aeration and surface fluctuations in moderate-slope stepped chute: from aeration inception to fully developed aerated flow, J. Hydraulic Res., IAHR 60 (6) (2022) 944–958.
[66] I.R. Wood, Air Water Flows, in: Proc. 21st IAHR Biennial Congress, Keynote address, Melbourne, Australia, 1985, pp. 18–29.
[67] I.R. Wood, Air Entrainment in Free-Surface Flows. IAHR Hydraulic Structures Design Manual No. 4, Hydraulic Design Considerations, Balkema Publ., Rotterdam, The Netherlands, 1991, p. 149.
[68] F. Zabaleta, F.A. Bombardelli, J.P. Toro, Towards an understanding of the mechanisms leading to air entrainment in the skimming flow over stepped spillways, Environ. Fluid Mech. 20 (2020) 375–392, https://doi.org/10.1007/s10652-019-09729-2.
[69] G. Zhang, Free-Surface Aeration, Turbulence, and Energy Dissipation on Stepped Chutes with Triangular Steps, Chamfered Steps, and Partially Blocked Step Cavities. Ph.D. thesis, The University of Queensland, School of Civil Engineering, 2017, p. 361, https://doi.org/10.14264/uql.2017.906.
[70] G. Zhang, H. Chanson, Interactions between free-surface aeration and total pressure on a stepped chute, Exp. Therm. Fluid Sci. 74 (2016) 368–381, https://doi.org/10.1016/j.expthermflusci.2015.12.011.
[71] G. Zhang, H. Chanson, Self-aeration in the rapidly- and gradually-varying flow regions of steep smooth and stepped spillways, Environ. Fluid Mech. 17 (1) (2017) 27–46, https://doi.org/10.1007/s10652-015-9442-z.
[72] G. Zhang, H. Chanson, H. Wang, Total pressure fluctuations and two-phase flow turbulence in self-aerated stepped chute flows, Flow Meas. Instrum. 51 (2016) 8–20, https://doi.org/10.1016/j.flowmeasinst.2016.08.007. ISSN 0955-5986.
[73] M. Hino, A Theory of the Mechanism of Self-Aerated Flow on Steep Slope Channels. Applications of the Statistical Theory of Turbulence. Technical Report C-6101, Technical Laboratory, Central Research Institute of Electric Power Industry, Japan, 1961, 42 pages.
[74] K.J. Sene, Aspects of Bubbly Two-Phase Flow, Ph.D. thesis, Trinity College, Cambridge, UK, December, 1984.